JOURNAL OF MECHANICAL ENGINEERING AND SCIENCES
ISSN: 2289-4659 e-ISSN: 2231-8380
VOLUME 9, ISSUE 3, 2025, 10770 - 10781
DOI: https://doi.org/10.15282/jmes.19.3.2025.6.0844

RESEARCH ARTICLE

Dynamic and sensitivity analysis of V-shaped cross-section piezoelectric beam as mass sensor for high-order vibration modes

H. Safari, R. Ghaderi*

Department of Mechanical Engineering, Shk.C., Islamic Azad University, Shahrekord, Iran

ABSTRACT - Resonators represent a new generation of sensors with superior performance and high sensitivity, making them well-suited for mass sensing applications. While V-shaped cross-section beams have demonstrated enhanced particle absorption and improved performance over conventional rectangular beams in the first bending mode, their behavior in higher-order vibration modes, including lateral bending, torsion, and in-plane bending, remains unexplored. This study presents a dynamic model of the vibratory motion of V-shaped beams after particle adsorption, employing both modal analysis and finite element methods. A sensitivity analysis based on Sobol's method is conducted to evaluate the influence of beam geometry on resonance frequency shifts post-adsorption and to quantify the extent of this effect. Simulation results reveal that V-shaped cross-section beams exhibit superior performance compared to rectangular beams, not only in the fundamental bending mode but also in higher-order vibration modes, including lateral bending, torsion, and in-plane bending. These findings highlight the potential of V-shaped resonators for advanced mass-sensing applications requiring multi-mode vibrational sensitivity.

ARTICLE HISTORY
Received : 27th Feb. 2025
Revised : 13th June 2025
Accepted : 02nd Sept. 2025
Published : 30th Sept. 2025

KEYWORDS
V-shape
Mass sensor
Piezoelectric beam
Vibration modes
Sensitivity analysis

1. INTRODUCTION

Nowadays, resonators are widely used in biosensing [1, 2], mass sensors [3, 4], elements of vibration in electrical circuits [5], and quantum coupling [6]. One of the most common applications of mechanical resonators is particle detection. In mass sensors, an adsorptive analyte on the upper surface of the microcantilever (MC) enables the absorption of polymer molecules and living cells. The adsorptive analyte was placed on the symmetry axis of the MC so that particle absorption would only affect the flexural vibration of the MC with no torsional motion. The great sensitivity of resonators introduced them as a new generation of mass sensors. Since these sensors do not require sample ionization and fragmentation for detecting biological substances, they are ideal for identifying viruses and bacteria [7, 8]. If particle absorption on the sensor is done thoroughly and completely, as the mass and the created surface tension increase, the sensor's stiffness, as well as its effective mass, also change. However, if particle absorption is done locally, only the mass of the sensor increases, which consequently decreases the resonance frequency of the sensor in different oscillation modes [9]. Thus, the change in resonance frequency in different oscillation modes is considered a suitable parameter for measuring the absorbed mass. Therefore, the greater the variations in the sensor's resonance frequency after particle absorption, the better the sensor's performance when used as a mass sensor. So far, many studies have been conducted to increase the frequency sensitivity of cantilevers as mass sensors, some of which include: reducing the geometric dimensions of the cantilever [10, 11], using carbon nanotubes [12, 13], and using different geometric shapes of the cantilever [14, 15]. One method that has received considerable attention is the use of various geometric shapes for the cantilever. Xu et al. [16] initially used simple rectangular and slotted cantilevers for aerosol particle mass sensing. To enhance the frequency sensitivity of the beam, they investigated different geometric dimensions of the beam. They determined the aspect ratios of length-to-width and width-to-thickness for these types of beams. Upadhyaya et al. [17] employed rectangular and triangular microcantilevers as mass sensors to study cancerous cells. Using the finite element method (FEM), they simulated surface stress on the microcantilever after cell adsorption. Additionally, the finite-difference time-domain (FDTD) method was utilized to extract the transmission characteristics of the photonic resonator structure. Their results demonstrated a pressure sensitivity of 60 nm/MPa for the triangular microcantilever profile. Nyang'au et al. [18] employed rectangular-shaped microcantilevers and arrow-shaped microcantilevers (a combination of rectangle and triangle) as mass sensors. They utilized these types of microcantilevers to detect physical, chemical, and biological particles. By using the novel microcantilever design, they achieved a sensitivity of 0.13 Hz/pg. Saiz et al. [19] simulated two types of triangular and arched triangular beams as mass sensors for absorbing biological particles and chemical agents, and compared their performance with that of rectangular beams. The simulation results showed that the selected beams had higher sensitivity in both coated and uncoated modes compared to the rectangular one. Using the finite element method, Niklin and Darabkhani investigated a U-shaped cantilever microbeam as a mass sensor and examined the effect of geometric dimensions on the sensor's performance [20].

In addition to single-layer mass sensors, which typically require an external actuator for vibrational excitation, piezoelectric beams represent another generation of mass sensors. By integrating a piezoelectric layer onto these beams,

*CORRESPONDING AUTHOR | R. Ghaderi | ✉ reza.ghaderi@iau.ac.ir

not only is the sensor's response speed enhanced, but miniaturization of the sensor is also achieved. Guo et al. [21], Pang et al. [22], and Qian et al. [23] used piezoelectric beams as mass sensors. Joshi et al. [24] experimentally tested a mass sensor excited by a piezoelectric layer on its top and concluded that the sensor's sensitivity increases with a reduction in the length of the piezoelectric layer. Niranjan et al. [25] used a piezoelectric beam as a mass sensor to detect SARS-CoV-2. Chauhan and Ansari [26] dynamically modeled three types of cantilevers of rectangular, stepped-rectangular, and stepped-triangular, in both air and vacuum environments. They employed a piezoelectric layer on the beam to excite vibrational motion and investigated resonant frequency variations in mass sensors using both experimental and analytical methods. The simulation results demonstrated that the triangular beam exhibits higher frequency sensitivity compared to the other two models. In addition to modifying the geometry of piezoelectric beams, altering the cross-sectional geometry of the base layer can also impact the frequency sensitivity of the beams by increasing their bending stiffness. This aspect has not been explored in previous studies on this type of beam. Although various geometric shapes of cantilevers have been employed in previous studies, the beam's cross-section has consistently been assumed to be rectangular. The effect of flexural rigidity resulting from changes in the cross-sectional geometry has not been investigated. Furthermore, the studies have predominantly considered only the first vibration mode as the operational mode. In contrast, the impact of higher-order vibration modes on the sensitivity of such sensors has not been explored. In vibrational motions, in addition to flexural vibration modes, torsional and in-plane modes also exist. However, the frequency sensitivity of these modes in mass sensors after particle adsorption has not been investigated so far.

Given the satisfactory performance of piezoelectric beams as mass sensors, and considering that the effect of cross-sectional area variation on the beam's frequency sensitivity, as well as the performance of the mass sensor in higher oscillation modes, torsional vibration modes, and in-plane modes, has not yet been investigated, this paper examines the behavior of the sensor in different oscillation modes by modifying the beam's cross-sectional geometry to enhance its bending stiffness. Additionally, a sensitivity analysis is conducted on the beam to evaluate the influence of geometric dimensions on its performance. To increase the beam stiffness and enhance the performance of the piezoelectric beam, a V-shaped cross-section is used instead of a rectangular one, as proposed by Gao et al. [27]. Applying the analytical method of modal analysis and the numerical method of finite element, the behavior of the V-shaped piezoelectric beam in lateral bending, torsion, and in-plane bending modes in different oscillation modes is investigated, and the performance of the V-shaped cross-section beam is compared with that of the conventional rectangular beam. Finally, to investigate how the geometric dimensions of the beam influence the variations in resonance frequency after particle absorption, a sensitivity analysis is conducted using Sobol's method.

2. MATERIAL AND METHODS

2.1 Dynamic Modeling of a Piezoelectric Beam

Cantilever beams are considered efficient tools when used as mass sensors. These types of sensors operate mainly based on the changes in the beam resonance frequency after particle absorption. To eliminate the effects of torsion and create a pure bending movement in these types of sensors, particle absorption is performed along the axis of symmetry. So far, most mass sensors have been rectangular cross-section cantilever beams, in which mass detection sensitivity and measurement accuracy depend on the beam's effective mass, resonance frequency, and analyte position. To enhance the performance of the beam as a mass sensor, a V-shaped beam is employed, which is excited by a piezoelectric layer on its top. Particle absorption is done on the longitudinal axis of symmetry and at the bottom of the V-shaped cross-section. According to Figure 1(a), the length of the beam consists of two parts: the beam with a piezoelectric layer of length L_1 and a single layer of length L_2. The rectangular cross-section of the piezoelectric layer has a width and thickness of W_p and hp, respectively. The V-shaped section has two flat flanges, W_1 and W_2. The groove part has a depth of H and a width of W. The thickness of the beam in the V-shaped section is h. To compare the performance of the V-shaped cross-section beam with that of the rectangular cross-section, the rectangular beam in Figure 1(b) is considered.

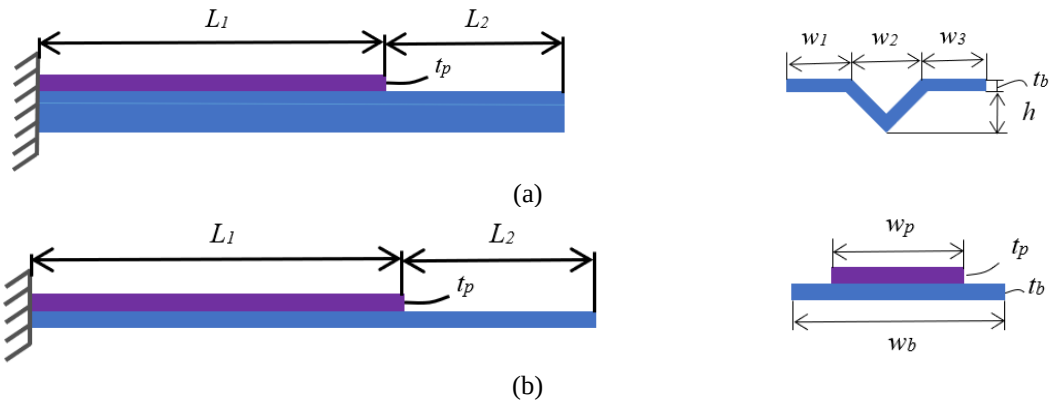

Figure 1. Schematic of: (a) V-shaped cross-section beam and (b) rectangular cross-section beam

By substituting Eqs. (A.1) and (A.5) in the Lagrange equation (see Appendix), the differential equation of the beam vibratory motion is obtained:

$$m(x)v''(x,t) + [K(x)v''(x,t)]'' + C_P''(x,t) = 0 \tag{1}$$

Furthermore, the relevant boundary conditions are:

$$\begin{aligned} x = 0: \quad & v(0,t) = 0,\ v'(0,t) = 0 \\ x = L: \quad & E_b I_b v''(L,t) + m_p \omega^2 v(L,t) = 0,\ v'''(L,t) = 0 \end{aligned} \tag{2}$$

In this equation, m_p is the mass of the particle added to the beam.

2.2 Analysis Modal of Differential Equation of Motion

To solve the linear differential equation of vibratory motion, Eq. (1), the Galerkin separation of variables method can be used:

$$v(x,t) = \sum_{n=1}^{\infty} \varphi_n(x) q_n(t) \tag{3}$$

where $\phi_n(x)$ is the nth mode shape and $q_n(t)$ is the time-dependent generalized coordinate. Considering the geometric discontinuity of the beam due to the existence of the piezoelectric layer, it can be divided into two uniform beams. Thus, the equation of the mode shapes is stated as follows:

$$\varphi_n(x) = \begin{cases} c_{11}\, Sin\, \beta_n x + c_{12}\, Cos\, \beta_n x + c_{13}\, Sinh\, \beta_n x + c_{13}\, Cosh\, \beta_n x & 0 < x < L_1 \\ c_{21}\, Sin\, \beta_n x + c_{22}\, Cos\, \beta_n x + c_{23}\, Sinh\, \beta_n x + c_{23}\, Cosh\, \beta_n x & L_1 < x < L_2 \end{cases} \tag{4}$$

The unknown coefficients of the equation, cij$\sqrt[4]{\frac{m\omega_n^2}{K}}$ can be obtained using the beam boundary conditions (Eq. (2)), continuity conditions, and normalization conditions with respect to mass. Based on the beam boundary and continuity conditions, the characteristic matrix equation of the system can be stated as follows:

$$J \times [c_{11} \quad c_{12} \quad c_{13} \quad c_{14} \quad c_{21} \quad c_{22} \quad c_{23} \quad c_{24}] = 0 \tag{5}$$

where, J is the characteristic matrix given by:

$$J = \begin{bmatrix} 0 & 1 & 0 & 1 \\ 1 & 0 & 1 & 0 \\ sin(\beta_n L_1) & cos(\beta_n L_1) & sinh(\beta_n L_1) & cosh(\beta_n L_1) \\ cos(\beta_n L_1) & -sin(\beta_n L_1) & cosh(\beta_n L_1) & sinh(\beta_n L_1) \\ -\gamma_1 sin(\beta_n L_1) & -\gamma_1 cos(\beta_n L_1) & \gamma_1 sinh(\beta_n L_1) & \gamma_1 cosh(\beta_n L_1) \\ -\gamma_1 cos(\beta_n L_1) & \gamma_1 sin(\beta_n L_1) & \gamma_1 cosh(\beta_n L_1) & \gamma_1 sinh(\beta_n L_1) \\ 0 & 0 & 0 & 0 \\ 0 & 0 & 0 & 0 \end{bmatrix}$$

$$\begin{bmatrix} 0 & 0 & 0 & 0 \\ 0 & 0 & 0 & 0 \\ -sin(\alpha_2 \beta_n L_1) & -cos(\alpha_2 \beta_n L_1) & -sinh(\alpha_2 \beta_n L_1) & -cosh(\alpha_2 \beta_n L_1) \\ -\alpha_2\, cos(\alpha_2 \beta_n L_1) & \alpha_2\, sin(\alpha_2 \beta_n L_1) & -\alpha_2\, cosh(\alpha_2 \beta_n L_1) & -\alpha_2\, sinh(\alpha_2 \beta_n L_1) \\ {\alpha_2}^2 sin(\alpha_2 \beta_n L_1) & {\alpha_2}^2 cos(\alpha_2 \beta_n L_1) & -{\alpha_2}^2 sinh(\alpha_2 \beta_n L_1) & -{\alpha_2}^2 cosh(\alpha_2 \beta_n L_1) \\ {\alpha_2}^3 cos(\alpha_2 \beta_n l_1) & -{\alpha_2}^3 sin(\alpha_2 \beta_n L_1) & -{\alpha_2}^3 cosh(\alpha_2 \beta_n L_1) & -{\alpha_2}^3 sinh(\alpha_2 \beta_n L_1) \\ -sin(\alpha_2 \beta_n L) & -cos(\alpha_2 \beta_n L) & sinh(\alpha_2 \beta_n L) & cosh(\alpha_2 \beta_n L) \\ -cos(\alpha_2 \beta_n L) + M_1 & sin(\alpha_2 \beta_n L) + M_2 & cosh(\alpha_2 \beta_n L) + M_3 & sinh(\alpha_2 \beta_n L) + M_4 \end{bmatrix} \tag{6}$$

where,

$$\alpha_2 = \sqrt[4]{\frac{m_p K_1}{(m_p + m_b) K_2}};\ \gamma_1 = \frac{K_1}{K_2} \tag{7}$$

$$\begin{aligned} M_1 = \frac{m_p}{m_b} \beta \alpha_2\, sin\, \alpha_2\, \beta L;\ M_2 = \frac{m_p}{m_b} \beta \alpha_2\, cos\, \alpha_2\, \beta L; \\ M_3 = \frac{m_p}{m_b} \beta \alpha_2\, sinh\, \alpha_2\, \beta L;\ M_4 = \frac{m_p}{m_b} \beta \alpha_2\, cosh\, \alpha_2\, \beta L \end{aligned} \tag{8}$$

To obtain the non-trivial solution for the matrix Eq. (5), the determinant of the matrix of coefficients J must be zero. By setting the determinant of the matrix J equal to zero, the value of β_n is obtained for different oscillation modes. To find β_n and, therefore, the post-adsorption natural frequency, Dekker's algorithm [28] was employed in MATLAB.

The MC resonant frequency in air due to system damping can be written as:

$$\omega_d = \omega_n \sqrt{1 - \xi^2} \tag{9}$$

where, ω_d is the damped resonance frequency, while ξ is the MC damping ratio in air. It is very complicated to determine ξ in a double-layer V-shaped MC. As particle absorption in MCs alters the natural frequency ω_n by changing the MC mass, it is possible to evaluate the vibration behavior of the MC after particle absorption and the MC resonant frequency by analyzing the alteration of the natural frequency [27].

The ordinary differential equation of the MC vibration motion is obtained by inserting v(x,t) from Eq. (3) in Eq. (1) (i.e., the differential motion equation), multiplying the equation by $\varphi_n(x)$, and integrating along the beam:

$$\ddot{q}_n + \omega_n^2 q_n + \sum_{m=1}^{\infty} C_{nm}\dot{q}_n + \gamma_n P(t) = 0 \tag{10}$$

where,

$$\omega_n^2 = \int_0^L \varphi_n(x)\frac{d^2}{dx^2}\left(K(x)\frac{d^2\varphi_n(x)}{dx^2}\right)dx \tag{11}$$

$$C_{nm} = \int_0^L C\varphi_n(x)\varphi_m(x)\,dx \tag{12}$$

$$\gamma_n = \int_0^{L_1} \varphi_n(x)\frac{d^2C_p(x)}{dx^2}dx \tag{13}$$

Numerical methods can be employed to solve Eq. (10). To this end, the Runge-Kutta method was used and programmed in MATLAB software.

3. RESULTS AND DISCUSSION

3.1 Dynamic Simulation of Piezoelectric Beam as Mass Sensor

To simulate the vibration motion of the V-shaped piezoelectric MC as a mass sensor, an MC with a piezoelectric layer on the upper surface was considered, as shown in Figure 1. The MC was assumed to have one fixed end and one free end. To evaluate the effects of adsorbed particles on MC vibration, particles were assumed to be adsorbed onto the free end of the MC. To investigate the pure flexural vibration, particle adsorption onto the axis of symmetry was assumed. Table 1 provides the geometric parameters and physical properties of the MC layers.

Table 1. Geometric characteristics and physical properties of the beam

	L_1 (mm)	L_2 (mm)	t (mm)	$w_{1,3}$ (mm)	w_2 (mm)	h (mm)	E (GPa)	ρ (kg/m^3)
V-shaped base layer	12	8	0.07	1	2	1	200	7800
Rectangular base layer	12	8	0.07	1	-	-	200	7800
Piezoelectric Layer	12	-	0.25	-	-	-	61	7650

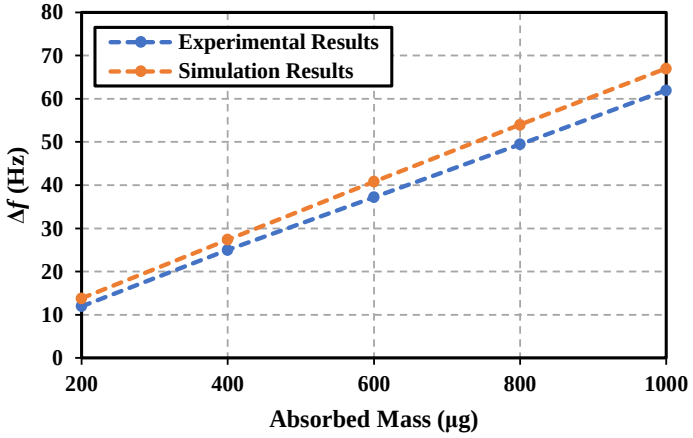

Figure 2. Effect of particle absorption on V-shaped beam natural frequency

To validate the dynamic simulation results of the piezoelectric beam as a mass sensor, the experimental results obtained by Gao et al. [27] were utilized. To that end, masses of 200, 400, 600, 800, and 1000 µg are placed on the beam tip and on its axis of symmetry in five different cases, and the beam resonance frequency is measured. In Figure 2, the variations in the V-shaped piezoelectric beam resonance frequency after particle absorption in the dynamic simulation

are compared with the practical results. The MC natural frequency changes upon the adsorption of particles. The pre- and post-adsorption natural frequencies of the MC could be obtained by solving the determinant of the coefficients of matrix J (Equation 6) for a certain adsorbed mass. The pre-adsorption natural frequency can be calculated using Equation 6, with m_p set to 0 in Equations 8 and 9. The difference between the pre- and post-adsorption natural frequencies gives the frequency shift. Figure 2 depicts the frequency shift for the adsorbed mass. As experimental data had been reported for the first mode [27], the frequency shift for the first mode was calculated. The results show a good agreement between the dynamic simulation results and the practical ones, with an average difference of only about 7.8% between the results in the five examined cases.

In mass sensors, the stiffness of the beam plays a crucial role in determining the sensor's performance. Therefore, to increase the stiffness of the beam, a V-shaped section, rather than a rectangular cross-section, was used in the base layer. To compare the performance of this beam as a mass sensor in higher oscillation modes (the first three modes) with that of a rectangular beam, according to Table 1, the two selected beams are considered to have the same length, width, thickness, and material. The absorbed mass is considered at the beam tip. After mass absorption, the variations in resonance frequency and oscillation amplitude for the first three modes of the two selected beams are compared. V-shaped MCs have a larger second moment of area than rectangular MCs. This results in higher stiffness and, consequently, a higher natural frequency. The V-shaped MC with a higher natural frequency experienced a larger change in its natural frequency than the rectangular MC upon the adsorption of particles. This contributes to the performance enhancement of the MC as a mass sensor. In general, MC stiffness enhancement in mass sensors would be an effective technique to improve sensor performance [27, 29], as shown in Figure 3. Particle absorption causes more frequency variations in all the first three oscillation modes of the V-shaped beam compared to the rectangular beam, indicating that the V-shaped beam exhibits better frequency performance in these modes as a mass sensor.

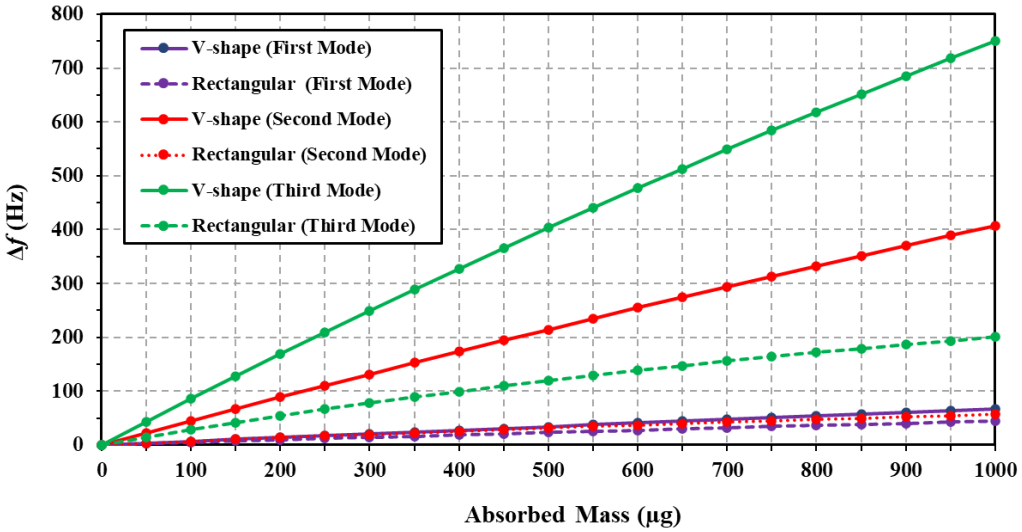

Figure 3. Frequency variations for the first three oscillation modes of the V-shaped beam and the rectangular beam

Figure 4 shows that particle absorption on the beam alters its effective mass, which affects both the resonance frequency and the amplitude of vibration across all three modes. Therefore, in addition to the resonance frequency, the amplitude of the vibratory motion can be used as a good parameter to detect the absorbed mass. Examining the beam frequency response before and after particle absorption in the first three oscillation modes reveals that, with the absorption of 1 μg of mass, the resonance frequencies in the first, second, and third modes change by 2.7%, 3.75%, and 2.55%, respectively. The highest and lowest frequency variations are observed in the second and first modes, respectively. Furthermore, the amplitude variations of the beam in the first, second, and third modes are 5.68%, 13.51%, and 0.34%, respectively, indicating that the highest amplitude variation is observed in the second mode. Therefore, it can be concluded that among the first three oscillation modes, the second mode is the most suitable, considering the performance of this beam as a mass sensor. A comparison of the post-adsorption vibration amplitude variation to the natural frequency implies that the vibration amplitude of the V-shaped MC had higher performance than the natural frequency parameter.

Table 2 compares the resonance frequency and oscillation amplitude variations of the V-shaped and rectangular beams after particle absorption in the first three modes. As can be seen, the variations of frequency to the absorbed mass in the V-shaped beam in the first, second, and third modes are 1.5, 7.2, and 3.75 times that of the rectangular beam, respectively, and the V-shaped beam amplitude variations in the first three oscillation modes are 3.20, 3.19, and 3.04 times that of the rectangular beam, respectively. Therefore, it can be concluded that the V-shaped beam exhibits better performance than the rectangular beam in terms of both amplitude and frequency variations. The V-shaped beam exhibits better performance and a more pronounced response as a mass sensor than the rectangular beam. Based on the results in Table 2, it can also be concluded that among the first three modes, the V-shaped beam exhibits better performance in the second oscillation mode in the frequency domain.

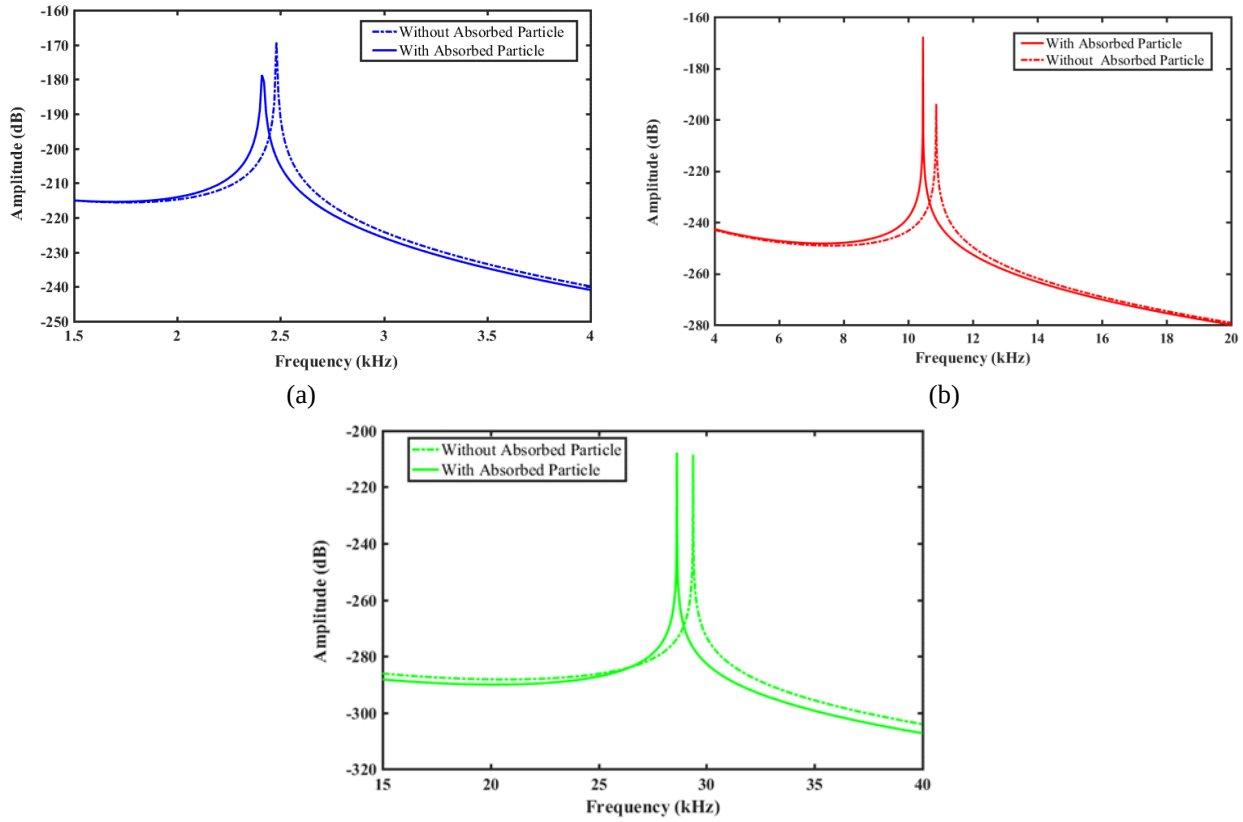

Figure 4. Frequency response of piezoelectric beam: (a) first mode, (b) second mode, and (c) third mode

Table 2. Effect of mass absorption on the resonance frequency and oscillation amplitude

	ΔA/Δm (db/μg)		*Δf/Δm (Hz/μg)*	
Section Type	V-shaped	Rectangular	V-shaped	Rectangular
First Mode	0.0096	0.003	0.067	0.0447
Second Mode	0.0262	0.0082	0.4077	0.0567
Third Mode	0.0070	0.0023	0.7507	0.2003

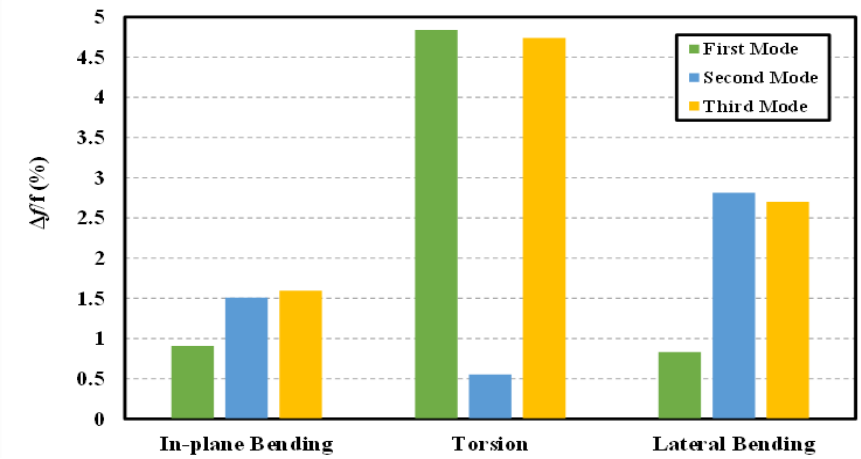

Figure 5. Effect of mass absorption on V-shaped piezoelectric beam vibration modes

Mass sensors can be used not only in lateral bending but also in torsional vibration and in-plane bending. Due to the complexity of modeling V-shaped beams under torsional and in-plane bending vibrations, the finite element method is employed to investigate their performance as mass sensors in these vibration modes. To that end, the selected beams were simulated using Abaqus software [30]. To simulate the double-layer MC, its components were drawn in three dimensions. Then, they were assembled using the tie module, ensuring no relative movement occurred between the two layers. The left corner of the MC was fully fixed, and the natural frequencies of the MC were calculated using the natural frequency module. 3D elements were employed to mesh the MC. The convergence was achieved with 23100 quadratic 3D stress

elements. The results obtained from the Abaqus software and analytical simulation for lateral bending (Figure 5) show that the highest frequency variations of the V-shaped cross-section beam in torsion, in-plane bending, and lateral bending occur in the third, first, and second modes, respectively

To compare the behavior of the V-shaped beam and rectangular beam in torsion and in-plane bending, the results of Figure 6 can be used. According to the results obtained in Figure 6(a), the in-plane bending frequency after mass absorption in the V-shaped beam has changed by 48%, 60%, and 134% in the first, second, and third modes, respectively, which is greater than that of the rectangular beam. Furthermore, according to Figure 6(b), in torsion, the frequency of the V-shaped beam has increased by 36%, 1%, and 7.58% in the first, second, and third modes, respectively, compared to the rectangular beam. This can be attributed to the higher lateral flexural stiffness and torsional stiffness of the V-shaped MC compared to the rectangular MC. These results also indicate that the V-shaped beam performs better than the rectangular beam in the first three oscillation modes of planar bending and torsion.

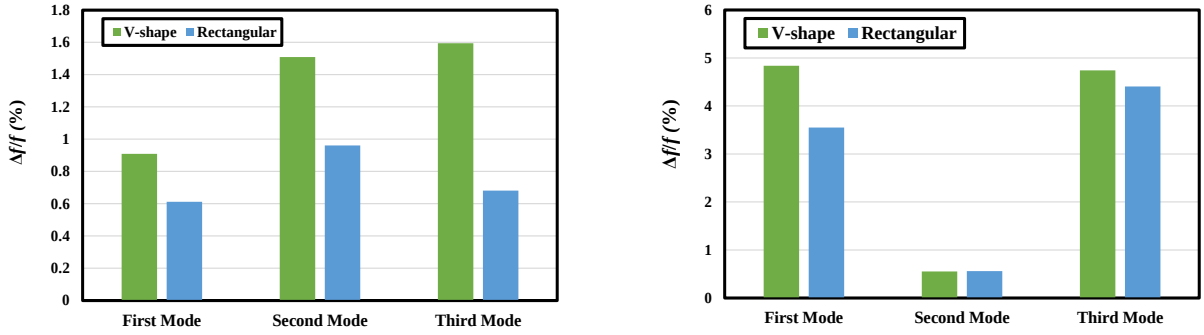

Figure 6. Comparing the effect of mass absorption on: (a) in-plane and (b) torsion vibration modes of V-shaped and rectangular section beams

3.2 Sensitivity Analysis of the Beam's Natural Frequency

The effect of the beam's geometric parameters on its resonance frequency variation after particle absorption (Δf) is a critical issue in studying the behavior of piezoelectric beams, as well as in designing them as a mass sensor. Obviously, the geometric parameters that significantly affect the beam resonance frequency can be considered the main parameters in developing this type of beam as a mass sensor. In the present study, to achieve the desired performance of the sensor, a sensitivity analysis of the piezoelectric beam's geometric dimensions is performed on the resonance frequency. To that end, Sobol's statistical method is used. The alteration of the MC natural frequency upon particle adsorption is dependent on the MC dimensions, i.e., the length, width, and thickness of each layer. Sobol's method would be efficient for analyzing the effects of these geometric parameters on the alteration of the natural frequencies, given the influences of all geometric parameters on target parameters (such as the natural frequency) [31-33]. Based on this method, arrays of input parameters (geometric dimensions of the beam) are formed, and then the target quantity (variations in the beam's resonance frequency) is calculated. Sensitivity analysis is performed to determine the effect of geometric parameters on variations in resonance frequency.

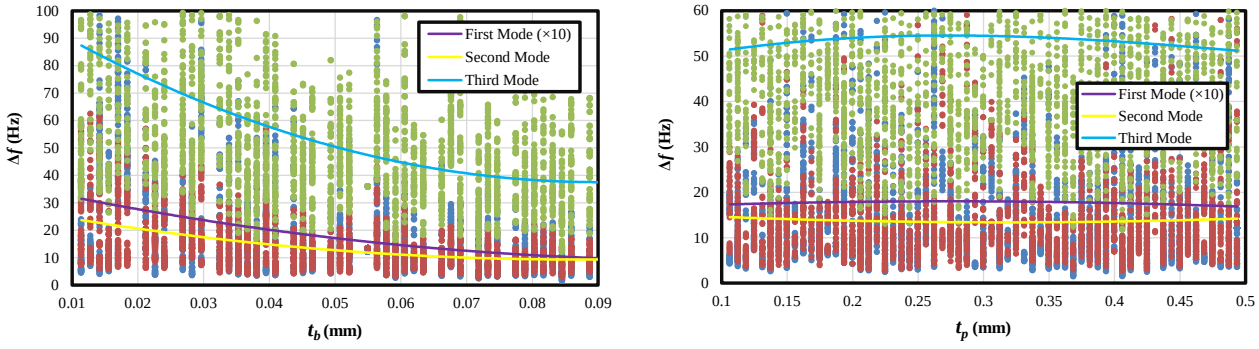

Figure 7. Effect of thickness of piezoelectric beam layers on resonance frequency: (a) base layer and (b) piezoelectric layer

Figure 7 shows how the thickness of the beam piezoelectric layer and base layer affects the beam resonance frequency variations after particle absorption in the first three oscillation modes. As can be seen, increasing the thickness of the piezoelectric layer in the first two modes, unlike the thickness of the beam base layer, which decreases Δf, does not significantly affect the variations in the beam resonance frequency after particle absorption compared to the first and second modes. This occurs during the third oscillation mode at t_p = 0.26 mm, where the value of Δf is maximized,

indicating optimal sensor performance at this value. In addition to the thickness of the beam layers, the width of the layers can affect Δf. Figure 8 shows the effect of the width parameter on Δf in the first three vibration modes of the beam. The results of Figure 8(a) show that the increase in the width of the flanges in the second and third modes exhibits an upward trend in intensity, which is more pronounced in the third period. Nonetheless, in the first mode, the value of Δf is minimized when w_1 = 1.55 mm. That is to say, this value of w_1 is considered the most inappropriate design value. Furthermore, according to Figure 8(b), the minimum values of w_2 (groove width) in the first to third modes of oscillation occur for values of 4.1, 4.25, and 3.9 mm, respectively, which are inappropriate values of w_2 in designing the beam.

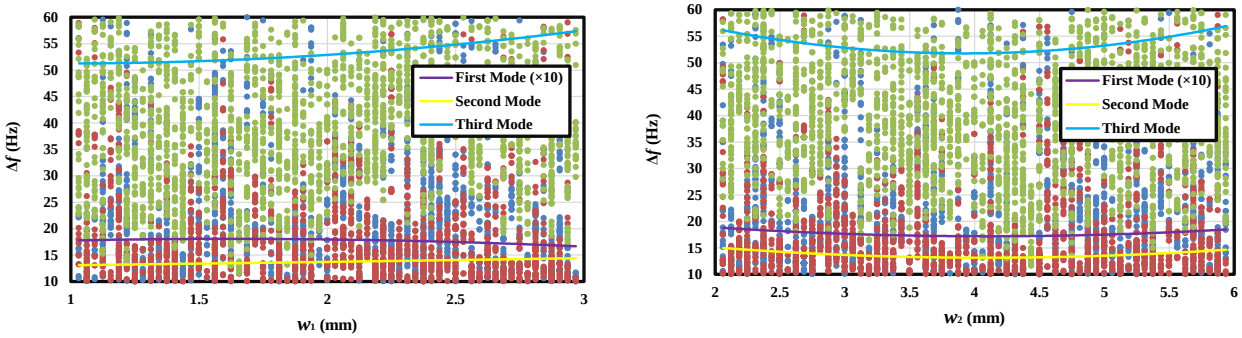

(a) (b)

Figure 8. Effect of width on resonance frequency: (a) flange width and (b) groove width

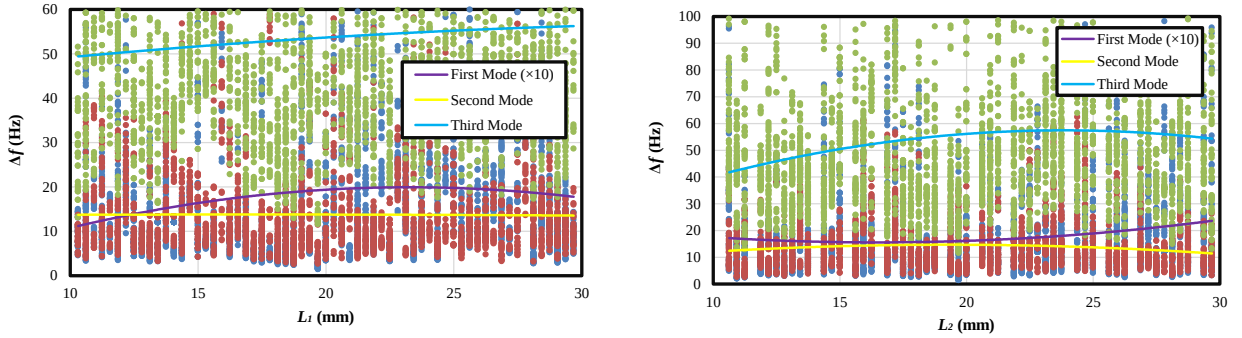

(a) (b)

Figure 9. Effect of piezoelectric beam length on resonance frequency: (a) piezoelectric layer and (b) extended area

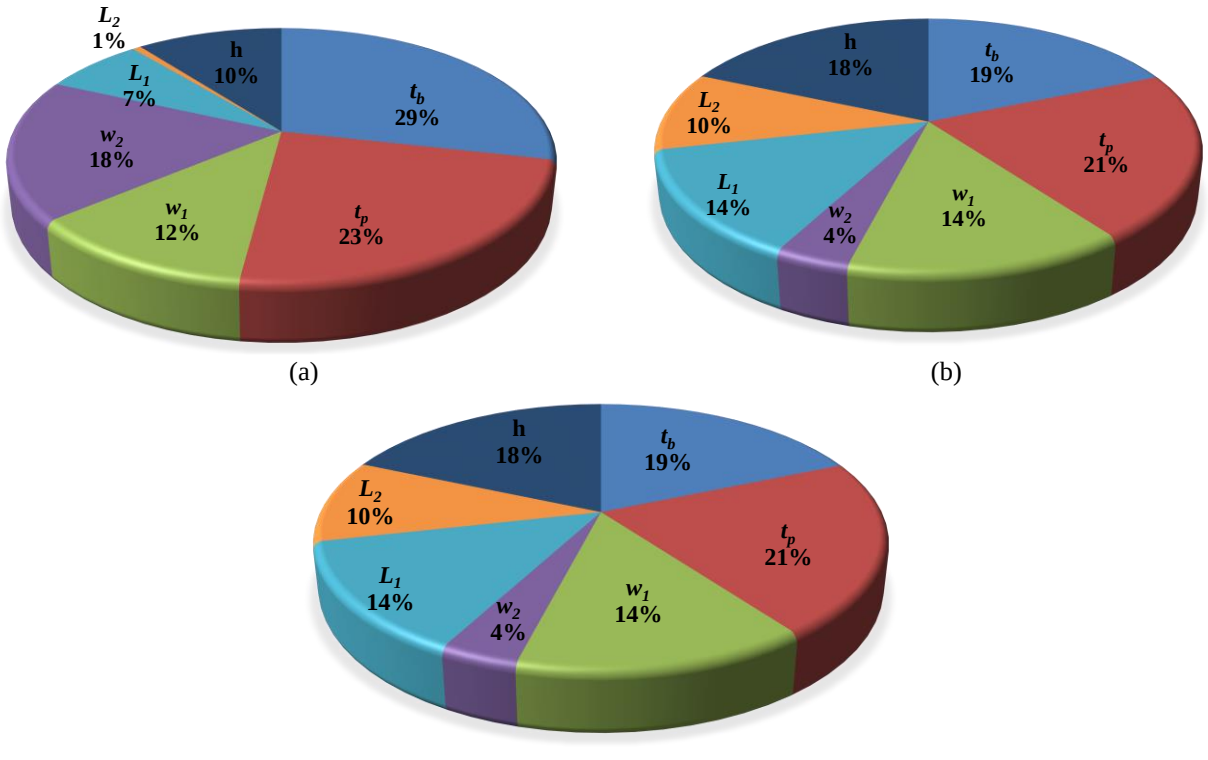

(a) (b)

(c)

Figure 10. Level of influence of geometric parameters on Δf in: (a) first mode, (b) second mode, and (c) third mode

Figure 9 shows the effect of the length of the piezoelectric layer and the extended beam on Δf. According to Figure 9(a), as the length of the piezoelectric layer increases in the second and third modes, Δf has a downward and upward trend, respectively. However, in the first oscillation mode, the value of Δf for L_1 = 23 mm reaches its maximum value, which is the optimal amount for design purposes. As the length increases, frequency variations decrease. According to Figure 9(b), for the extended length of 16.5mm, the value of Δf is minimized in the first oscillation mode, and it is maximized in the second and third oscillation modes for the lengths of 18 and 23.8 mm, respectively. Therefore, the appropriate and inappropriate values of designing the extended length in the first three modes of oscillation are determined. The Sobol sensitivity analysis allows not only for assessing how different parameters affect the target but also for measuring these effects. In other words, the parameters with the most significant impact on the target can be identified. The frequency shift upon particle adsorption was the target, and the Sobol sensitivity analysis was employed to find the geometric parameters with the most significant effects on the frequency shift. Each geometric parameter contributes to the frequency shift; these contributions were measured through Sobol sensitivity analysis on a scale of 0-100% for comparison purposes. Figure 10 shows the sensitivity of Δf to the geometric dimensions of the beam and the piezoelectric layer in the first three oscillation modes. As can be seen, the thickness of the piezoelectric layer and the base layer are the most influential geometric parameters on Δf when designing this type of beam as a mass sensor. Nonetheless, the length of the piezoelectric layer in the first mode and the base layer's groove width in the second and third oscillation modes have a minimal effect on Δf.

4. CONCLUSIONS

To increase the sensitivity of piezoelectric beams as a mass sensor, a V-shaped cross-section was used instead of a rectangular cross-section. Since in resonators, the absorbed mass is determined based on the variations in the resonance frequency, the variations in the resonance frequency of the V-shaped cross-section beam after particle absorption were dynamically modeled using modal and finite element analysis methods, and the performance of this type of beam was compared to that of the rectangular one. The geometric dimensions of the beam influence the shift in resonance frequency (Δf) after particle absorption. Sobol's sensitivity analysis was used to quantify the extent of this influence. The results of dynamic modeling and sensitivity analysis of the beam show that:

i) Among the first three oscillation modes, the V-shaped cross-section piezoelectric beam shows the highest amplitude and frequency variations after particle absorption in the second mode, indicating the better performance of this beam as a mass sensor in the second oscillation mode.

ii) Comparing the performance of the V-shaped beam with the rectangular one reveals that the most significant difference between the beams occurs in the second and first oscillation modes, as reflected in the frequency variations after particle absorption and the amplitude of vibratory motion, respectively.

iii) Abaqus software simulation results also show the better performance of the V-shaped cross-section beam compared to the rectangular one, such that the variations of resonance frequency in torsional and in-plane vibration in the first and third modes are 1.36 and 2.34 times, respectively, as great as those of the rectangular beam.

iv) The results of the sensitivity analysis using Sobol's method show that the thickness of the piezoelectric layer and base layer are the most influential geometric parameters on Δf in the first three oscillation modes, respectively. Moreover, these geometric parameters are the most important ones in designing this type of beam as a mass sensor.

ACKNOWLEDGMENTS

This study was not supported by any grants from funding bodies in the public, private, or not-for-profit sectors.

CONFLICT OF INTEREST

The authors declare that they have no conflicts of interest.

AUTHORS CONTRIBUTION

H. Safari (Methodology; Data curation; Formal analysis; Visualization; Writing -original draft)

R. Ghaderi (Methodology; Data curation; Formal analysis; Visualization; Writing -original draft)

AVAILABILITY OF DATA AND MATERIALS

The data supporting this study's findings are available on request from the corresponding author.

ETHICS STATEMENT

The authors have not employed an AI-based tool or AI technology to write this article.

REFERENCES

[1] H. Sharifi, S. Eskandari, "Sensing blood components and cancer cells with photonic crystal resonator biosensor. *Results in Optics*, vol. 14, p. 100593, 2024.

[2] H. Bahri, A. Hocini, H. Bensalah, S. Mouetsi, S. Ingebrandt, V. Pachauri, et al., "A high-sensitivity biosensor based on a metal–insulator–metal diamond resonator and application for biochemical and environmental detections," *Optik*, vol. 271, p. 170083, 2022.

[3] W. Yu, A. Banerjee, J. Hirotani, T. Tsuchiya, "Enhancing responsivity and detection limit in tunable nano-electromechanical system resonator mass sensors," *Japanese Journal of Applied Physics*, vol. 63, no. 3, p. 03SP74, 2024.

[4] X. Xiao, S.-C. Fan, C. Li, "The effect of edge mode on mass sensing for strained graphene resonators," *Micromachines*, vol. 12, no. 2, p. 189, 2021.

[5] D. Sank, M. Khezri, S. Isakov, J. Atalaya, "Balanced coupling in electromagnetic circuits," *Physical Review Applied*, vol. 23, no. 2, p. 024012, 2025.

[6] B. Harpt, J. Corrigan, N. Holman, P. Marciniec, D. Rosenberg, D. Yost, et al., "Ultra-dispersive resonator readout of a quantum-dot qubit using longitudinal coupling," *npj Quantum Information*, vol. 11, no. 1, p. 5, 2025.

[7] S. Bannur Nanjunda, V. N. Seshadri, C. Krishnan, S. Rath, S. Arunagiri, Q. Bao, et al., "Emerging nanophotonic biosensor technologies for virus detection," *Nanophotonics*, vol. 11, no. 22, p. 5041–5059, 2022.

[8] Z. Jiang, B. Feng, J. Xu, T. Qing, P. Zhang, Z. Qing, "Graphene biosensors for bacterial and viral pathogens," *Biosensors and Bioelectronics*, vol. 166, p. 112471, 2020.

[9] V. Puerto-Belda, J. J. Ruz, C. Millá, Á. Cano, M. L. Yubero, S. García, et al., "Measuring vibrational modes in living human cells," *PRX Life*, vol. 2, no. 1, p. 013003, 2024.

[10] M. Katta, R. Sandanalakshmi, V. Veerraju, "Microcantilever geometry analysis for array sensor design," *Materials Today: Proceedings*, vol. 50, p. 1496–1501, 2022.

[11] H. Darban, "Size effect in ultrasensitive micro-and nanomechanical mass sensors," *Mechanical Systems and Signal Processing*, vol. 200, p. 110576, 2023.

[12] H. Chen, M. Xiao, J. He, Y. Zhang, Y. Liang, H. Liu, et al., "Aptamer-functionalized carbon nanotube field-effect transistor biosensors for Alzheimer's disease serum biomarker detection," *ACS Sensors*, vol. 7, no. 7, p. 2075–2083, 2022.

[13] H. M. Sedighi, M. Malikan, "Stress-driven nonlocal elasticity for nonlinear vibration characteristics of carbon/boron-nitride hetero-nanotube subject to magneto-thermal environment," *Physica Scripta*, vol. 95, no. 5, p. 055218, 2020.

[14] M. Xiao, C. Xia, D.F. Wang, "A mass-position sensing scheme using a geometrically adjustable resonator with low-order modals for detecting multiple analytes," *IEEE Transactions on Instrumentation and Measurement*, vol. 72, p. 1–12, 2023.

[15] R. Perelló-Roig, S. Barceló, J. Verd, S. Bota, J. Segura, "Geometrically engineered mass sensing CMOS-MEMS resonators for temperature compensation via folded anchors," *Sensors and Actuators A: Physical*, vol. 373, p. 115435, 2024.

[16] F. Xu, Y. Wei, S. Bian, H. Wang, D.-R. Chen, D. Kong, "Simulation-based design and optimization of rectangular micro-cantilever-based aerosols mass sensor," *Sensors*, vol. 20, no. 3, p. 626, 2020.

[17] A. M. Upadhyaya, M. C. Srivastava, P. Sharan, "Integrated MOEMS-based cantilever sensor for early detection of cancer," *Optik*, vol. 227, p. 165321, 2021.

[18] W. O. Nyang'au, A. Setiono, A. Schmidt, H. Bosse, E. Peiner, "Sampling and mass detection of a countable number of microparticles using on-cantilever imprinting," *Sensors*, vol. 20, no. 9, p. 2508, 2020.

[19] P. G. Saiz, D. Gandia, A. Lasheras, A. Sagasti, I. Quintana, M. I. Arriortua, et al., "Enhanced mass sensitivity in novel magnetoelastic resonators geometries for advanced detection systems," *Sensors and Actuators B: Chemical*, vol. 296, p. 126612, 2019.

[20] D. Nicklin, H. Gohari Darabkhani, "Design, modelling, and experimental validation of a glass U-tube mass sensing cantilever for particulate direct-on-line emissions measurement," *Atmosphere*, vol. 14, no. 6, p. 915, 2023.

[21] K. Guo, B. Jiang, B. Liu, X. Li, Y. Wu, S. Tian, et al., "Study on the progress of piezoelectric microcantilever beam micromass sensor," in *IOP Conference Series: Earth and Environmental Science*, vol. 651, p. 022091, 2021.

[22] J. Pang, X. Le, K. Pang, Z. Xu, C. Gao, J. Xie, "Modified coefficient of equivalent mass to explain decreased relative sensitivity of piezoelectric cantilever humidity sensor in high mode," *Journal of Microelectromechanical Systems*, vol. 29, no. 4, p. 452–454, 2020.

[23] J. Qian, H. Begum, J. E.-Y. Lee, "Acoustofluidic localization of sparse particles on a piezoelectric resonant sensor for nanogram-scale mass measurements," *Microsystems & Nanoengineering*, vol. 7, no. 1, p. 61, 2021.

[24] P. Joshi, S. Kumar, V. K. Jain, J. Akhtar, J. Singh, "Distributed MEMS mass-sensor based on piezoelectric resonant micro-cantilevers," *Journal of Microelectromechanical Systems*, vol. 28, no. 3, pp. 382–389, 2019.

[25] A. Niranjan, P. Gupta, M. Rajoriya, "Piezoelectric MEMS micro-cantilever biosensor for detection of SARS–CoV–2," in *2021 International Conference on Communication, Control and Information Sciences (ICCISc)*, pp. 1-5, 2021.

[26] S. Chauhan, M. Z. Ansari, "Vacuum-assisted piezoelectric cantilever mass sensor performance," *Journal of Mechanical Science and Technology*, vol. 35, pp. 5489–5494, 2021.

[27] R. Gao, Y. Zhang, J. Zhao, S. Liu, "A novel V-shaped cross-section cantilever sensor for monitoring concentrated masses with improved detecting sensitivity and measuring accuracy," *IEEE Sensors Journal*, vol. 14, no. 2, pp. 514–521, 2013.

[28] R. P. Brent. Algorithms for Minimization without Derivatives. 1st Ed. New York: Courier Corporation, 2013.

[29] J. Zhao, R. Gao, S. Liu, Y. Huang, "A new sensitivity-improving method for piezoelectric resonance mass sensors through cantilever cross-section modification," *IEEE Transactions on Industrial Electronics*, vol. 61, no. 3, pp. 1612–1621, 2013.

[30] F. Hejazi, H. M. Esfahani. Interpretive Solutions for Dynamic Structures Through ABAQUS Finite Element Packages. 1st Ed. Boca Raton: CRC Press, 2021.

[31] H. Korayem, R. Ghaderi, "Sensitivity analysis of nonlinear vibration of AFM piezoelectric microcantilever in liquid," *International Journal of Mechanics and Materials in Design*, vol. 10, no. 2, pp. 121–131, 2014.

[32] R. Ghaderi, B. M. Dehkordi, A. R. Fard, "Vibration and sensitivity analysis of double-layered non-uniform piezoelectric microcantilever as a self-sensing mass sensor*," Physica Scripta*, vol. 96, no. 11, p. 115205, 2021.

[33] M. Korayem, M. Taheri, S. Ghahnaviyeh, "Sobol method application in dimensional sensitivity analyses of different AFM cantilevers for biological particles," *Modern Physics Letters B*, vol. 29, no. 22, p. 1550123, 2015.

APPENDIX

To dynamically model the V-shaped cross-section and rectangular cross-section beams, the Euler-Bernoulli theory method is employed. To that end, the beam kinetic energy is:

$$T = \frac{1}{2}\int_0^L m(x)\dot{v}(x,t)^2 dx \tag{A.1}$$

where $v(x,t)$ is the bending deformation of the beam at a point x and time t. L indicates the total length of MC (L_1+L_2), and $m(x)$ is the mass per unit length of the beam, which is as follows in the two areas of the beam:

$$m(x) = \left(m_b + m_p\right)\left(H_0 - H_{L_1}\right) + m_b\left(H_{L_1} - H_L\right) \tag{A.2}$$

where, $H(x)$ is the Heaviside function and is defined as H_L=$H(x$-$L)$ and m_b and m_p are:

$$\begin{aligned} m_b &= \rho_b t_b (w_1 + w_3 + \sqrt{w_2^2 + 4h^2}) \quad \text{for a V-shaped section} \\ m_b &= \rho_b w_b t_b \quad \text{for rectangular section} \end{aligned} \tag{A.3}$$

$$m_p = \rho_p w_p t_p \quad \text{for V-shaped and rectangular sections} \tag{A.4}$$

where ρ_b and ρ_p are the densities of the base layer and that of the piezoelectric layer, respectively. Since energy is a scalar quantity, the total potential energy of the bending beam is obtained by summing the potential energies of the base layer and the piezoelectric layer. Since the strain in pure bending of the beam is considered one-dimensional (ε_{yy}=ε_{xy}=0), the strain potential energy can be written as $U = \frac{1}{2}\int_0^L \iint_A \sigma_{xx}\varepsilon_{xx} dA dx$. According to the theory of beams, due to the small deformations along the thickness and width of the beam, the effect of Poisson's ratio can be ignored. Therefore, the longitudinal strain is defined as $\varepsilon_{xx} = -y v_{xx}$. On the other hand, the utilized piezoelectric layer undergoes bending vibration when an alternating potential difference is applied to both sides and is used as a source of vibration force for the beam. According to the basic equation of piezoelectric materials, the stress created in the piezoelectric layer as a result of applying electric voltage $P(t)$ in one-dimensional axial form can be written as $\sigma_p = E_p\varepsilon_p - E_p d_{31} P(t)$. Therefore, the beam's total potential energy is calculated as follows:

$$U = \frac{1}{2}\int_0^L (K(x)v''^2(x,t) + C_P(x,t)v''(x,t))dx \tag{A.5}$$

where $K(x)$ and C_p are the equivalent bending stiffness of the beam and the electromechanical coupling coefficient of the piezoelectric layer, respectively, which are as follows for the whole beam:

$$K(x) = K_1(H_0 - H_{L_1}) + K_2(H_{L_1} - H_L) \tag{A.6}$$

$$C_P = E_P d_{31} w_P \left(y_n + 0.5t_p\right) P(t) \left(H_0 - H_{L_1}\right) \tag{A.7}$$

in which:

For V-shaped section:

$$\begin{aligned} K_1 = E_b \Big[& I_b + w_1 h (t_{n1} - \frac{t_b}{2})^2 + w_2 (h + t_b)(\frac{h + t_b}{2} - t_{n1})^2 - \frac{w_2 h}{2}(\frac{h}{3} - t_{n1})^2 \; - \frac{w_2 h}{2}(\frac{2h}{3} + t_b - t_{n1})^2 \\ & + w_3 h (t_{n1} - \frac{t_b}{2})^2) \Big] + E_p w_p t_p \left[\frac{{t_p}^2}{12} + (t_{n1} + \frac{t_p}{2})^2 \right] \end{aligned} \tag{A.8}$$

$$\begin{aligned} K_2 = E_b \Big[& I_b + w_1 t_b (t_{n2} - \frac{t_b}{2})^2 + w_2 (h + t_b)(\frac{h + t_b}{2} - t_{n2})^2 - \frac{w_2 h}{2}(\frac{h}{3} - t_{n2})^2 \\ & - \frac{w_2 h}{2}(\frac{2h}{3} + t_b - t_{n2})^2 + w_3 t_b (t_{n2} - \frac{t_b}{2})^2) \Big] \end{aligned} \tag{A.9}$$

For Rectangular Section:

$$K_1 = E_b w_b t_b \left(\frac{1}{3} t_b^2 + t_n^2 - 2 t_b t_n\right) + E_p w_p t_p \left[\frac{1}{12} t_p^2 + \left(t_b + \frac{t_p}{2} - t_n\right)^2\right] \tag{A.10}$$

$$K_2 = \frac{1}{12} w_b t_b^3 \tag{A.11}$$

and intermediate variables I_b, t_{n1}, t_{n2} and t_n are:

$$I_b = \frac{1}{12}[(w_1 + w_3) t_b^3 + w_2 (h + t_b)^3] - \frac{1}{18} w_2 h^3 \tag{A.12}$$

$$t_{n1} = \frac{1}{2} \frac{E_p w_p t_p^2 - E_b \left[w_1 t_b^2 + w_2 (h + t_b)^2 - \frac{w_2 h^2}{3} - w_2 h (\frac{2h}{3} + t_b) + w_3 t_b^2 \right]}{E_p w_p t_p + E_b (w_1 + w_2 + w_3) t_b} \tag{A.13}$$

$$t_{n2} = \frac{1}{2} \frac{w_1 t_b^2 + w_2 (h + t_b)^2 - \frac{w_2 h^2}{3} - w_2 h (\frac{2h}{3} + t_b) + w_3 t_b^2}{(w_1 + w_2 + w_3) t_b} \tag{A.14}$$

$$t_n = \frac{1}{2} \frac{E_b w_b t_b^2 + E_p w_p t_p \left(2t_b + t_p\right)}{E_b w_b t_b + E_p w_p t_p} \tag{A.15}$$

In these equations, E_b and E_P are the modulus of elasticity of the base layer and piezoelectric layer, respectively